ACS OMEGA

Article

Cite This: ACS Omega 2018, 3, 167−175

Core−Shell Zeolitic Imidazolate Frameworks for Enhanced Hydrogen Storage

Dharmendra K. Panchariya,[†] Rohit K. Rai,[‡] E. Anil Kumar,*[,†,∥] and Sanjay K. Singh*[,‡,§]

[†]Discipline of Mechanical Engineering, [‡]Discipline of Chemistry, and [§]Discipline of Metallurgy Engineering and Materials Science, Indian Institute of Technology Indore, Simrol, Indore 453552, India

[∥]Department of Mechanical Engineering, Indian Institute of Technology Tirupati, Tirupati 517506, India

Supporting Information

ABSTRACT: Core−shell ZIF-8@ZIF-67- and ZIF-67@ZIF-8-based zeolitic imidazolate frameworks (ZIFs) were synthesized solvothermally using a seed-mediated methodology. Transmission electron microscopy−energy-dispersive X-ray spectrometry, line scan, elemental mapping, X-ray photoelectron spectroscopy, and inductively coupled plasma-atomic emission spectroscopy analyses were performed to confirm the formation of a core−shell structure with the controlled Co/Zn elemental composition of ∼0.50 for both the core−shell ZIFs. The synthesized core−shell ZIF-8@ZIF-67 and ZIF-67@ZIF-8 frameworks conferred enhanced H_2 (2.03 and 1.69 wt %) storage properties at 77 K and 1 bar, which are ca. 41 and 18%, respectively, higher than that of the parent ZIF-8. Notably, the distinctly remarkable H_2 storage properties shown by both the core−shell ZIFs over the bimetallic Co/Zn-ZIF and the physical mixture of ZIF-8 and ZIF-67 clearly evidenced their unique structural properties (confinement of porosity) and elemental heterogeneity due to the core−shell morphology of the outperforming core−shell ZIFs. Moreover, H_2 adsorption isotherm data of these frameworks are best fitted with the Langmuir model ($R^2 \geq 0.9999$). Along with the remarkably enhanced H_2 storage capacities, the core−shell ZIFs also displayed an improved CO_2 capture behavior. Hence, we demonstrated here that the controlled structural features endorsed by the rationally designed porous materials may find high potential in H_2 storage applications.

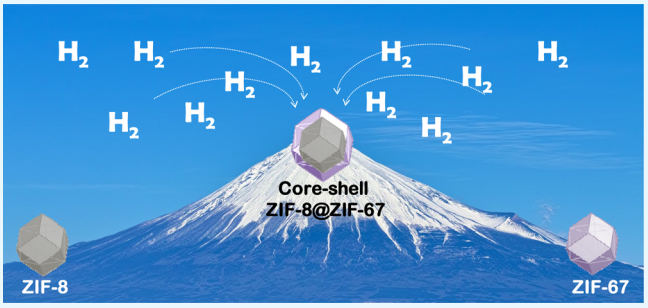

INTRODUCTION

In the present scenario of increasing world population, demand and consumption of natural energy resources (fossil fuels and gases) increase day by day, causing their rapid depletion. Hence, to meet the global demand in an environmentally benign way is to explore for new sustainable and clean energy resources such as H_2-based fuels.[1−3] To achieve these objectives, the recent development of porous crystalline materials attracted wide attention for H_2 storage. Among the most high-performing porous materials, metal organic frameworks (MOFs) generated great attention because of their exceptional physical and chemical characteristics such as high specific surface area, large porosity, and excellent thermal and chemical stability in various environments.[4,5] In this context, one of the widely explored MOFs is zeolitic imidazolate frameworks (ZIFs), as they find various advanced properties for diverse applications in energy storage, gas adsorption and separation, catalysis, and so on.[6−19] In the recent past, a wide range of chemically distinct ZIFs were investigated, in which ZIF-8 [$Zn(Hmim)_2$] and ZIF-67 [$Co(Hmim)_2$] frameworks have been extensively explored.[6,7,12,20,21] For gas storage applications over ZIFs, various strategies are explored to effectively fine-tune the morphology and topology of the ZIF structure. In this context, functionalization of organic linkers or post modification (composites) over single-metal ZIFs has been widely investigated, albeit with limited results.[6−9,13−19,22−25] Among several strategies, mixed metals or bimetallic MOFs designed by introducing new secondary metal ions/clusters into single-metal MOFs have been identified as one of the most facile routes to construct new materials with tuned properties. For instance, Botas et al. for the first time experimentally reported in situ substitution of Zn^{2+} ions in IRMOF-1 (MOF-5) by Co^{2+} (Co/Zn ≤ 1:4) and achieved higher adsorption capacities of H_2, CO_2, and CH_4 at a high pressure (up to 10 bar), where incorporation of Co^{2+} was expected to provide more assessable sites to gas molecules from unexposed metal sites.[26] Kuang et al. synthesized Co-doped ZnO ($Zn_{1-x}Co_xO$, x = 0.03, 0.05, and 0.10) for the development of diluted magnetic semiconductors.[27] Yamauchi et al. used a bimetallic ZIF (Co_x·$Zn_{1-x}(MeIm)_2$) as a template for the synthesis of highly porous carbon materials.[28] Recently, we have also synthesized highly robust bimetallic Co_xZn_{100-x}-ZIF-8 (x = 25, 50, and 75 and 90%), where $Co_{75}Zn_{25}$-ZIF-8 displayed superior H_2 and CO_2 uptakes at 77 and 298 K, respectively, at 1 bar. We

Received: November 1, 2017
Accepted: December 25, 2017
Published: January 5, 2018

DOI: 10.1021/acsomega.7b01693
ACS Omega 2018, 3, 167−175

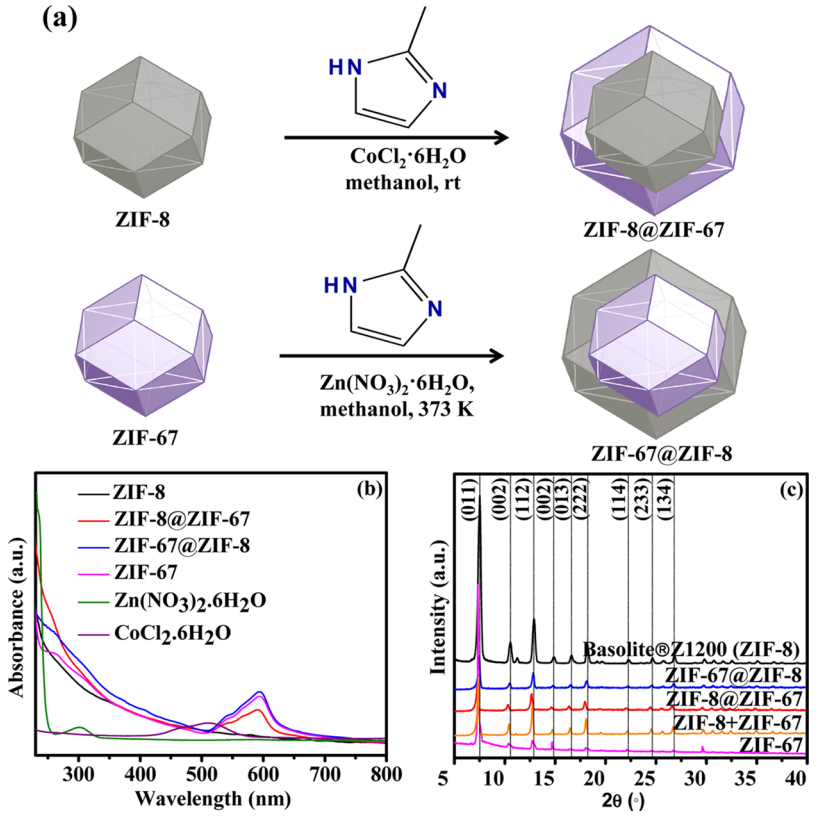

Figure 1. (a) Synthetic scheme of preparation of core−shell ZIF-8@ZIF-67 and ZIF-67@ZIF-8, (b) UV−visible spectra, and (c) powder X-ray diffraction (PXRD) patterns of ZIF-8, ZIF-67, ZIF-8@ZIF-67, ZIF-8 + ZIF-67, and ZIF-67@ZIF-8.

demonstrated that by varying the Co/Zn content in the bimetallic Co/Zn-ZIF, chemical heterogeneity and porosity can be fine-tuned and hence excellent gas uptake can be achieved.[29] Very recently, Verpoort et al. also reported similar bimetallic Zn/Co ZIFs for gas (N_2, CO_2, and CH_4) sorption applications and catalytic conversion of CO_2 to cyclic carbonates.[30] These recent findings displayed that bimetallic ZIFs possess improved physical and chemical properties compared to single-metal ZIFs, and therefore it is obvious to understand why these bimetallic ZIFs are being extensively explored for wide applications, including as potential materials for enhanced gas storage.[26−30] Despite these encouraging findings, there are several considerable challenges for the development and utilization of such bimetallic materials, as appropriately discussed by Xu et al., such as fragile yields of the framework, segregation of metals, and unpredicted topologies and functionalities of bimetallic MOFs for advanced applications in gas storage and separation.[31]

In contrary to bimetallic MOFs, core−shell MOFs have shown considerably high potential to overcome some of the above-highlighted challenges;[31] for instance, intrinsic structural components of the participating MOFs remain intact and well-understood for core−shell MOFs. Therefore, construction of such core−shell MOFs could be an effective alternative way to tune or introduce new fascinating properties in MOFs[32] and consequently to improve their performance for various advanced applications, in particular for gas storage and separation. Earlier reports in this direction demonstrated the potential of core−shell MOFs for wide applications.[32−39] Rosi et al. reported a porous bio-MOF-11/14@bio-MOF-14 framework, which exhibited an enhanced CO_2 uptake (58.3 $cm^3\ g^{-1}$) compared to the parent bio-MOF-14 (44.8 $cm^3\ g^{-1}$).[33] Facile construction of IRMOF-3@MOF-5 and MOF-5@IRMOF-3@MOF-5 and their reversed structures with a similar topology were also reported.[34] Szilágyi et al. described the synthesis of IRMOF-2@MOF-5 and Janus MOF-5@IRMOF-2 and vice versa and explored these MOFs for H_2 uptake (up to 25 bar).[35] Yamauchi et al. also constructed ZIF-8@ZIF-67 frameworks and utilized these frameworks as a template to synthesize functionalized nanoporous hybrid carbon materials for electrochemical analysis.[36] A similar ZIF-67@ZIF-8 framework was reported by Li et al., which was transformed into Pd@H−Zn/Co-ZIF to achieve an enhanced catalytic activity for semi-hydrogenation of acetylene.[37] Feng et al. described a new approach, instead of seed-mediated growth, for the construction of multilayered core−shell ZIF-8@ZIF-67 and ZIF-8@ZIF-67@ZIF-8 structures. They demonstrated that under controlled slow nucleation process, double-layered core−shell of ZIF-8@ZIF-67 and ZIF-67@ZIF-8 frameworks with a thick shell can be synthesized at room temperature.[38] Core−shell MIL-101@UiO-66 was also reported to show a significant enhancement in H_2 uptake (26 and 60%, as compared to the parent MIL-101 and UiO-66, respectively).[39] Although core−shell MOFs displayed significantly improved properties than the parent MOFs, surprisingly, application of core−shell ZIF@ZIF was not explored extensively for gas storage applications.

Herein, we synthesized core−shell ZIF-8@ZIF-67 and ZIF-67@ZIF-8 frameworks by a seed-mediated growth method while keeping a Co-to-Zn molar ratio of ∼0.50 for both the core−shell structures. Transmission electron microscopy (TEM) and scanning electron microscopy (SEM) images, TEM−energy-dispersive X-ray spectrometry (EDXS) line scanning, and elemental mapping were performed to establish the core−shell structures, whereas X-ray photoelectron spec-

DOI: 10.1021/acsomega.7b01693
ACS Omega 2018, 3, 167−175

troscopy (XPS) and inductively coupled plasma-atomic emission spectroscopy (ICP-AES) analyses confirmed the electronic state and the molar composition of Zn and Co elements in the core−shell ZIFs. Core−shell ZIFs possess unprecedented tuned framework properties (surface area, pore volume, and pore size distribution). Remarkably, enhanced H_2 storage properties were achieved over the core−shell ZIF-8@ZIF-67 and ZIF-67@ZIF-8 frameworks, which are significantly higher than those of the parent ZIF-8. The obtained experimental data were fitted well with the Langmuir adsorption equilibrium isotherm model. Moreover, the core−shell ZIF-8@ZIF-67 and ZIF-67@ZIF-8 frameworks also displayed improved CO_2 capture properties compared to either of the parent ZIFs. To the best of our knowledge, the observed impressive H_2 storage and improved CO_2 capture are amongst the best reported till date, within the analogous class of core−shell ZIFs.

RESULTS AND DISCUSSION

Synthesis and Morphology Characteristics of Core−Shell ZIFs. Core−shell ZIF-8@ZIF-67 and ZIF-67@ZIF-8 frameworks were synthesized by a seed-mediated growth methodology under solvothermal conditions, as illustrated in Figure 1a. Freshly prepared ZIF-67 seeds and commercially available ZIF-8 (Basolite Z1200) were used as seeds for the synthesis of core−shell ZIF-67@ZIF-8 and ZIF-8@ZIF-67 frameworks, respectively.[36,37] A visible color change from pale white for ZIF-8 to off-violet and dark violet for core−shell ZIF-67@ZIF-8 and ZIF-8@ZIF-67 frameworks, respectively, has also been observed during the synthesis of these core−shell ZIFs (Figure S1). The UV−vis absorption spectra (Figure 1b) well supported the formation of core−shell ZIF-8@ZIF-67 and ZIF-67@ZIF-8 frameworks, where the presence of characteristic bands for the tetrahedral Co^{2+} at ∼580 and ∼540 nm with no significant shift, compared to that of the parent ZIF-67, suggests the presence of Co^{2+} in the ZIF-8@ZIF-67 and ZIF-67@ZIF-8 frameworks.[29,37,40] Notably, the analogous isoreticular sodalite topology and similar unit cell parameters for ZIF-8 ($a = b = c$ = 16.9910 Å) and ZIF-67 ($a = b = c$ = 16.9589 Å) and comparable ionic radii of Zn^{2+} (0.74 Å) and Co^{2+} (0.72 Å) drive the facile synthesis of the core−shell ZIF-8@ZIF-67 and ZIF-67@ZIF-8 frameworks with a topology analogous to those of the parent ZIF-8 and ZIF-67.[9,12,20,27,29]

Figure 1c illustrates the PXRD patterns of the synthesized core−shell ZIFs along with those of the parent ZIF-8 and ZIF-67 (Figure S2). The presence of high-intensity peaks in the PXRD spectra is in good agreement with the highly crystalline nature of the synthesized core−shell ZIFs.[36−38] Diffraction peaks appeared at 2θ values of 7.52, 10.53, 12.90, 14.86, 16.60, 18.21, 22.21, 24.66, and 26.82° were identified for the (011), (002), (112), (002), (013), (222), (114), (233), and (134) planes, respectively.[29] The PXRD characteristics of the parent ZIF-8 (Basolite Z1200) resemble well the earlier reported PXRD patterns of Basolite Z1200 (Figures 1c and S3).[41] Notably, no additional phase was found, and the close resemblance of the PXRD diffraction peaks of the core−shell ZIFs with those of the parent ZIF-8 and ZIF-67 suggests that the intrinsic framework properties of the participating ZIF-8 and ZIF-67 remain intact during the formation of the core−shell ZIFs.[9,12,20,21,29] Moreover, the PXRD pattern of the physical mixture of ZIF-8 and ZIF-67 also showed diffractions peaks analogous to those of the parent ZIFs (Figure 1c). The TEM and SEM images established a well-defined rhombic dodecahedron topology with a uniform size distribution independently for both the core−shell ZIF-8@ZIF-67 and ZIF-67@ZIF-8 frameworks (Figures 2a,e and S4). TEM−

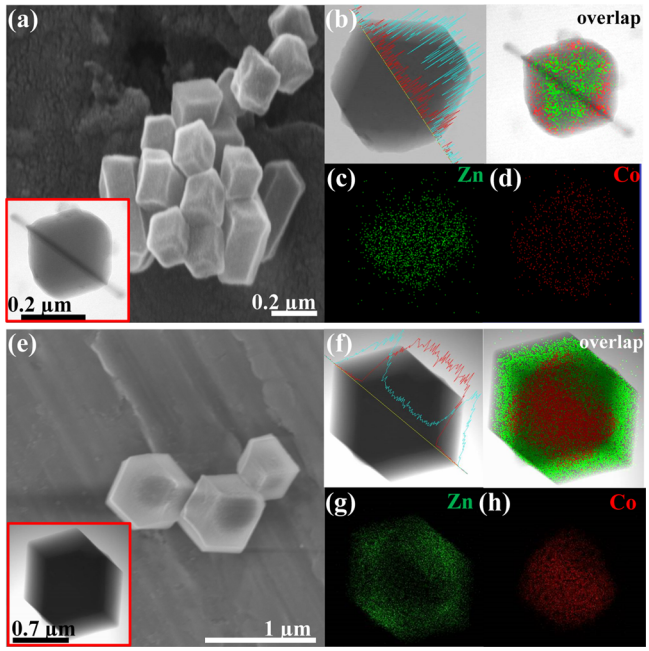

Figure 2. (a,e) SEM images (inset: TEM images), (b,f) line scanning, and (c,d,g,h) elemental mapping of (a−d) ZIF-8@ZIF-67 and (e−h) ZIF-67@ZIF-8 frameworks.

EDXS, line scan, and elemental mapping analyses further confirmed the composition and distribution of Zn and Co elements within the core−shell ZIFs (Figures 2b−d,f−h and S5). Distribution of Zn in the core and Co at the shell in ZIF-8@ZIF-67 and analogously Co in the core and Zn at the shell in ZIF-67@ZIF-8 clearly evidenced the core−shell frameworks of the synthesized ZIF-8@ZIF-67 and ZIF-67@ZIF-8 frameworks.[36−38] Despite the fact that ZIF-67@ZIF-8 has a larger particle size than ZIF-8@ZIF-67, the core-to-shell thickness ratio was observed to be comparable for both the core−shell ZIFs (Table S1).

Moreover, ICP-AES analysis also authenticated the comparable Co-to-Zn molar ratio for both core−shell ZIF-8@ZIF-67 (Co/Zn = 0.51) and ZIF-67@ZIF-8 (Co/Zn = 0.54). XPS analysis was performed to establish the electronic states of Co and Zn elements present in the core−shell ZIF-8@ZIF-67 and ZIF-67@ZIF-8 frameworks (Figures 3a,d, S6, and S7 and Table S2). The high-resolution spectra of Zn 2p (∼1021 eV) and Co 2p (∼781 eV) were in good agreement with those of the Zn^{2+} and Co^{2+} oxidation states (Figure 3b,c,e,f). Moreover, the signals corresponding to Co^{2+} appeared to be of low intensity, suggesting the presence of Co (ZIF-67) in the core of ZIF-67@ZIF-8. Analogously, for ZIF-8@ZIF-67, the signals for Zn^{2+} were found to be of lower intensity because of the encapsulation of ZIF-8 in the ZIF-67 shell.[27,37] The N 1s peak at ∼399 eV was assigned to the N atom of the 2-methylimidazole linker (Figures S6d and S7d). Moreover, an elemental analysis also confirms that almost similar wt % of C ≈ 48, N ≈ 23, and H ≈ 5.5 are present in ZIF-8@ZIF-67 and ZIF-67@ZIF-8 (Figure S8). Fourier transform infrared spectroscopy (FT-IR) vibration bands for ZIF-8@ZIF-67 and ZIF-67@ZIF-8 showed characteristics bands at ∼2929 and ∼1581

DOI: 10.1021/acsomega.7b01693
ACS Omega 2018, 3, 167−175

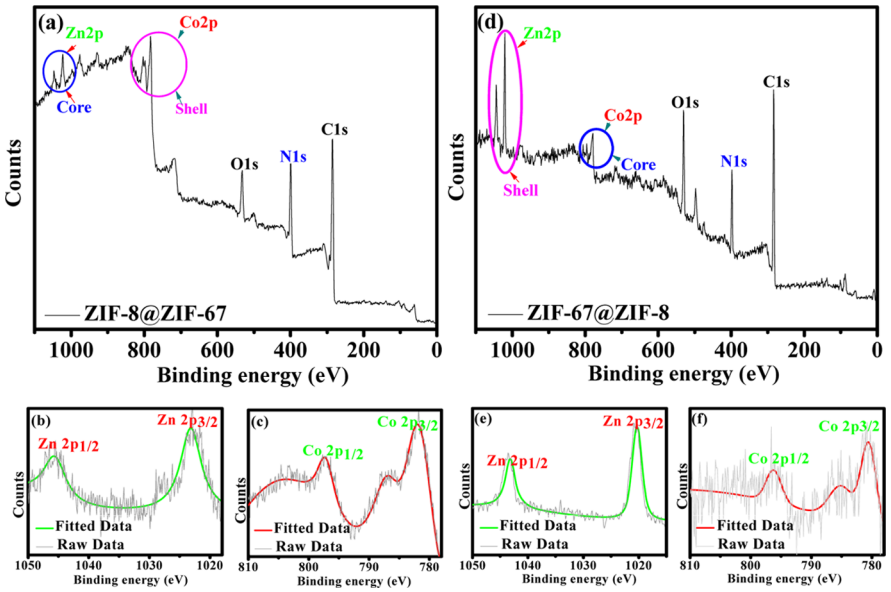

Figure 3. (a,d) Wide-scan XPS spectra and (b,c,e,f) respective high-resolution XPS spectra showing Zn 2p and Co 2p core bands of ZIF-8, ZIF-67, ZIF-8@ZIF-67, and ZIF-67@ZIF-8 frameworks.

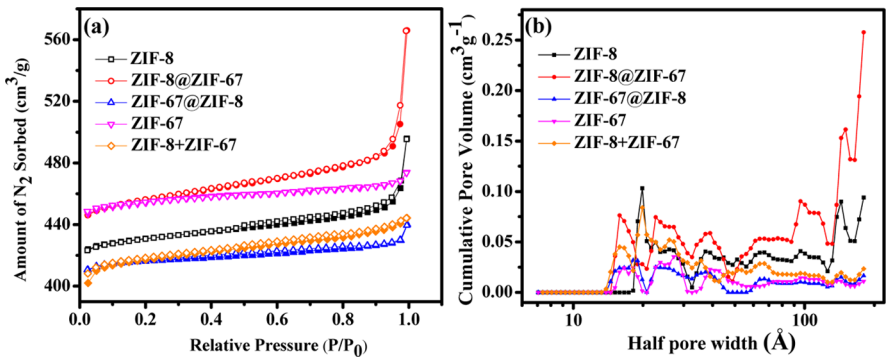

Figure 4. (a) N_2 sorption and (b) DFT pore size distribution of ZIF-8, ZIF-67, ZIF-67@ZIF-8, and ZIF-8 + ZIF-67 physical mixture frameworks.

Table 1. Surface Area, Pore Volume, Pore Size, and H_2 Storage Properties of the Core−Shell ZIF-8@ZIF-67 and ZIF-67@ZIF-8 Frameworks Along with Those of ZIF-8, ZIF-67, and ZIF-8 + ZIF-67 Physical Mixture

				H_2 uptake at 77 K, 1 bar		
ZIFs	surface area[a] ($m^2\ g^{-1}$)	pore volume[b] ($cm^3 g^{-1}$)	pore size[c] (nm)	mmol g^{-1}	wt %	references
ZIF-8	1323.62	0.7633	1.11	7.08	1.43	this work
ZIF-8@ZIF-67	**1402.15**	**0.8752**	**1.20**	**10.07**	**2.03**	**this work**
ZIF-67@ZIF-8	1271.82	0.6797	1.02	8.37	1.69	this work
ZIF-8 + ZIF-67	1295.64	0.6871	1.03	7.69	1.55	this work
ZIF-67	1392.30	0.7324	1.01	7.55	1.53	this work
$Co_{75}Zn_{25}$-ZIF-8	1571.7	0.7750	1.97	7.69	1.55	29

[a]BET surface area. [b]Total pore volume (estimated at P/P_0 = 0.99). [c]Average pore radius.

cm^{-1} assigned to the C−H and C═N banding vibrations, respectively, suggesting that the 2-methylimidazole linker remains intact during the formation of the core−shell ZIFs. Notably, the presence of a vibration band at ∼421 cm^{-1} corresponding to the Zn−N or Co−N bond stretching demonstrated the presence of Zn-imidazolate/Co-imidazolate linkage in the core−shell ZIFs (Figure S9).[37] Thermogravimetric analysis (TGA) curves of the ZIF-8@ZIF-67 and ZIF-67@ZIF-8 frameworks along with those of the parent ZIF-8 and ZIF-67 are shown in Figure S10. The TGA curves of ZIF-8 and ZIF-67 match well with the earlier reports.[9,12,20,21,29,36,37] Interestingly, core−shell ZIF-8@ZIF-67 and ZIF-67@ZIF-8 were thermally stable up to 370 and 340 °C, respectively, which is analogous to that of ZIF-67 (390 °C) but lower than that of ZIF-8 (410 °C). These results evidenced the presence of heterogeneity in the studied core−shell ZIF-8@ZIF-67 and ZIF-67@ZIF-8 frameworks.[33,36,37]

The surface area, total pore volume, and pore size distribution of core−shell ZIF-8@ZIF-67 and ZIF-67@ZIF-8 and the physical mixture of ZIF-8 and ZIF-67 frameworks were analyzed by measuring the N_2 adsorption−desorption isotherms at 77 K, where all studied ZIFs displayed type-I

DOI: 10.1021/acsomega.7b01693
ACS Omega 2018, 3, 167−175

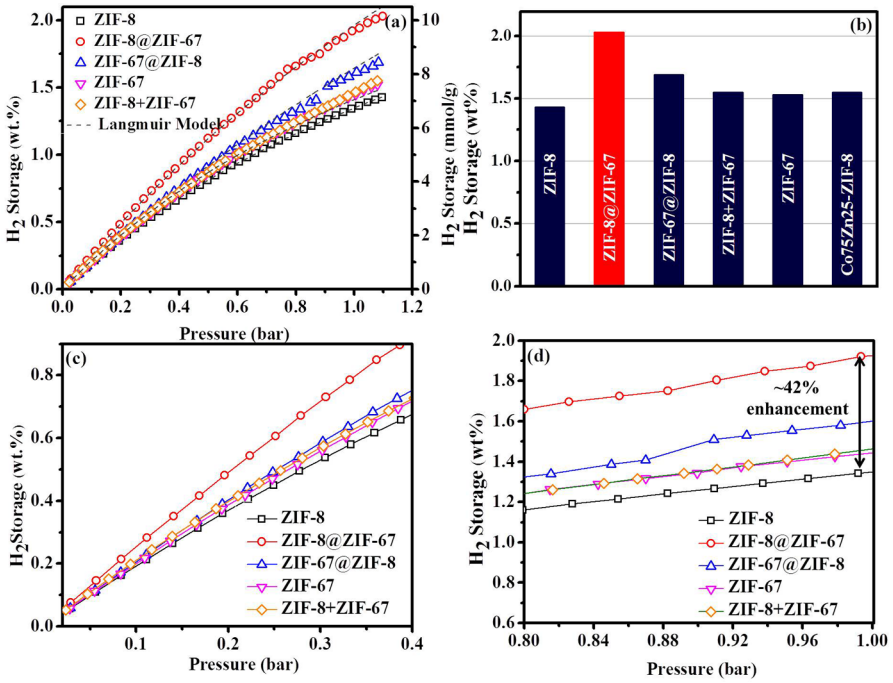

Figure 5. (a) H_2 storage isotherm at 77 K with a Langmuir model, (b) comparative H_2 storage, and (c,d) enlarged view of the H_2 storage isotherm in the pressure range of (c) 0.025−0.4 bar and (d) 0.80−1.0 bar.

isotherm (Figures 4a and S11 and Table 1). The pore size distributions were calculated by density functional theory (DFT) and Barrett−Joyner−Halenda (BJH) methods, as shown in Figures 4b and S12. It is also observed that the estimated average pore sizes of the ZIF-8@ZIF-67 (~ca. 1.20 nm), ZIF-67@ZIF-8 (~ca. 1.02 nm), and ZIF-8 + ZIF-67 (~ca. 1.03 nm) frameworks are almost similar to those of the parent ZIF-8 (~ca. 1.11 nm) and ZIF-67 (~ca. 1.01 nm).[9,10,12,20,21,29,36,37] Notably, the Brunauer−Emmett−Teller (BET) surface area (1402.15 $m^2\ g^{-1}$) and total pore volume of the ZIF-8@ZIF-67 framework structure showed an increment by ca. ~6% (5.93%) and ca. ~15% (14.66%), respectively, as compared to the parent ZIF-8. Such enhancement may be due to the well-grown ZIF-67 shell over the ZIF-8 core, without intercepting the pores of ZIF-8. In contrary, ZIF-67@ZIF-8 showed a lower BET surface area (1271.82 $m^2\ g^{-1}$) and total pore volume, ca. ~8.65 and ~ca. 7%, respectively, lower than those of the ZIF-67 core, presumably because of the blockage of the pore at the interface of the ZIF-8 shell and the ZIF-67 core. The BET surface area (1295.64 $m^2\ g^{-1}$) and total pore volume (0.6871 $cm^3\ g^{-1}$) of the physical mixture of ZIF-8 and ZIF-67 frameworks were almost similar to the average values of the parent ZIF-8 and ZIF-67. Hence, the above results clearly evidenced the distinct surface and porosity behavior of core−shell ZIF-8@ZIF-67 and ZIF-67@ZIF-8, due to their core−shell topology, compared to the parent ZIF-8 and ZIF-67 and the ZIF-8 + ZIF-67 physical mixture. The close agreement of the observed trend in the pore volume and pore size of the core−shell ZIFs with that of the respective core inferred the predominant role of the core in controlling the growth of the shell in accordance with the crystal lattice of the core.[32,33]

H_2 Storage Properties. Envisioned by the remarkably enhanced surface properties of the core−shell ZIF-8@ZIF-67 and ZIF-67@ZIF-8 frameworks, we explored the H_2 storage capacities of these frameworks. The H_2 adsorption isotherms were obtained at 77 and 298 K, respectively, in the pressure range of 0−1.0 bar (Figures 5a−d and S13 and Table 1). Interestingly, the ZIF-8@ZIF-67 and ZIF-67@ZIF-8 frameworks displayed enhanced H_2 storage capacities of 2.03 and 1.69 wt %, respectively, compared to the parent ZIF-8 (1.43 wt %) and ZIF-67 (1.53 wt %) at 77 K. Between both the studied core−shell ZIFs, the ZIF-8@ZIF-67 framework outperformed ZIF-67@ZIF-8 and showed a remarkable enhancement in the H_2 storage capacity by 41.95% than the core ZIF-8 and 32.68% more H_2 storage capacity than the shell ZIF-67. Interestingly, the surface area of the core−shell ZIF-8@ZIF-67 is almost analogous to that of the shell ZIF-67, whereas it is only 5.93% higher than that of the core ZIF-8. Notably, ZIF-67 having a surface area analogous to that of ZIF-8@ZIF-67 exhibited much lower H_2 storage properties, suggesting that presumably the porous ZIF-67 shell complemented well with the core ZIF-8 to facilitate the observed enhancement in the H_2 storage for core−shell ZIF-8@ZIF-67. In contrary, the other core−shell ZIF-67@ZIF-8 exhibited a lower H_2 storage than core−shell ZIF-8@ZIF-67 and only 10−18% higher H_2 storage than the core ZIF-67 and shell ZIF-8, suggesting that the shell ZIF-8 significantly prevented the H_2 uptake by the core. Moreover, the core−shell ZIF-8@ZIF-67 exhibited a distinctly enhanced H_2 storage even at the low pressure range of 0.025−0.4 bar, suggesting an efficient and rapid interaction of H_2 molecules with the micro−mesoporous surface of core−shell ZIF-8@ZIF-67 (Figure 5c). Further, it was also noted that the H_2 adsorption isotherm was not saturated within the investigated pressure range up to 1 bar (Figure 5d), suggesting that higher H_2 storage can be possible at a high pressure. Notably, ZIF-8@ZIF-67 and ZIF-67@ZIF-8 exhibited very low H_2 uptake values of 0.084 and 0.043 wt %, respectively, at 298 K up to 1 bar; nevertheless, the trend is consistent with that observed at 77 K (Figures 5 and S13). It should be noted that in general, MOFs exhibited a low H_2 uptake at 298 K even at a high pressure; for instance, Yildirim et al. reported 0.13 wt % over ZIF-8 at 30

DOI: 10.1021/acsomega.7b01693
ACS Omega 2018, 3, 167−175

bar; and therefore, at a low pressure and 298 K, there will be more uncertainty in the estimated H_2 uptake values.[42a]

Further, to validate if the observed H_2 storage performance of the core−shell ZIFs is due to the structural modification due to their core−shell morphology, the H_2 storage performance of the physical mixture of ZIF-8 and ZIF-67 (Co/Zn = 0.50) was also evaluated. It should be noted that the physical properties of the ZIF-8 + ZIF-67 physical mixture were found to be the average of those of the parent ZIF-8 and ZIF-67, and hence a similar trend was also expected for the H_2 storage properties of the ZIF-8 + ZIF-67 physical mixture. This was indeed the case, as the H_2 storage of the physical mixture of ZIF-8 and ZIF-67 (1.55 wt %) was found to be well below that of the high-performing core−shell frameworks (2.03 wt % for ZIF-8@ZIF-67) and is almost an average of those of ZIF-8 and ZIF-67. A similar behavior has also been observed by Rosi et al., where the core−shell II-bio-MOF-14 exhibited a 4-fold lower N_2 gas adsorption compared to the grinded II-bio-MOF-14, which was attributed to the exposure of the core to the N_2 gas upon grinding.[33] This further elaborated the advantage with the core−shell morphology, where the gas must pass through the shell before filling into the core.[33] Notably, the observed H_2 storage capacity of the core−shell ZIFs was also found to be higher than that of the bimetallic $Co_{75}Zn_{25}$-ZIF-8 (1.55 wt %) and comparable to those of most of the similar class of MOFs (Table S3).[29,31] The H_2 storage capacities were on the order of ZIF-8@ZIF-67 > ZIF-67@ZIF-8 > ZIF-8 + ZIF-67 > ZIF-67 > ZIF-8 (Table 1). Hence, the above observations clearly evidenced that the special arrangement of ZIF-8 and ZIF-67 in the core−shell topology is responsible for the observed increment in the H_2 adsorption properties of the studied core−shell ZIFs and not just because of the mere presence of the individual components (ZIF-8 and ZIF-67). Notably, no visible changes in the diffraction patterns were observed in the PXRD patterns of the core−shell ZIFs before and after gas adsorption, suggesting that their core−shell structures remain intact (Figure S14). Moreover, to know the adsorption behavior of H_2 molecules, Langmuir and Freundlich equations (Figures 5a and S15−S17 and Table S4) were applied to fit the experimental H_2 adsorption isotherms of ZIF-8@ZIF-67, ZIF-67@ZIF-8, ZIF-8, and ZIF-67 frameworks. The fitting parameters and represented correlation coefficients (R^2) inferred a good agreement of the experimental isotherm with the Langmuir model ($R^2 \geq 0.9999$) compared to the Freundlich model, suggesting that the H_2 adsorption behavior of the studied core−shell frameworks adopts the theoretically expected model.[43,44] Moreover, the estimated heat of adsorption (ΔH_{ads}) values were found to be ∼3.45 and ∼3.40 kJ/mol, respectively, for ZIF-8@ZIF-67 and ZIF-67@ZIF-8. Notably, the obtained ΔH_{ads} values were estimated over a large temperature difference (77−298 K) range and a low pressure range (0−1 bar) and therefore may led to an uncertainty in the estimated ΔH_{ads} values. Nevertheless, the estimated ΔH_{ads} values are in good agreement with the other literature findings (∼4.3 and ∼3.8 kJ/mol for MIL-101(Cr) and Li@AC-MIL-101-A, respectively, and ∼4.8 kJ/mol for ZIF-8).[42]

CO_2 Capture Properties. Encouraged by the observed noteworthy enhancement in H_2 storage capacities of the studied core−shell ZIF-8@ZIF-67 and ZIF-67@ZIF-8 frameworks, the performance of these core−shell ZIFs was also explored for CO_2 capture capacities at 298 K and 1 bar (Figure S18 and Tables S5 and S6). All ZIFs displayed a linear increase in the CO_2 adsorption capacities with the increase in pressure (0−1.0 bar). Consistent with the advancement in the surface and porosity properties of core−shell ZIF-8@ZIF-67 over the ZIF-67@ZIF-8 frameworks and the parent ZIF-8 and ZIF-67, a 2-fold increment in CO_2 capture capacities to 1.67 mmol g^{-1} (7.35 wt %) was observed for core−shell ZIF-8@ZIF-67 as compared to the core ZIF-8 (0.83 mmol g^{-1}, 3.65 wt %) and shell ZIF-67 (1.11 mmol g^{-1}, 4.91 wt %). Analogously, the other core−shell ZIF-67@ZIF-8 also exhibited 18.54% more CO_2 capture than the core ZIF-67 and 59.45% more CO_2 capture than the shell ZIF-8. Nevertheless, the studied core−shell ZIFs exhibited CO_2 capture capacities comparable or even superior to most of the bimetallic ZIFs or MOFs at 1 bar and 298 K (Table S7). Hence, the easily tunable structure of the core−shell frameworks by the critically chosen core and the shell materials and exploiting the complementary integration of the core to the shell, along with the other crucial factors such as surface functionalities, optimum porosity structure, interaction between gas molecules and pore wall, and the chemical heterogeneity of the core−shell frameworks, have a vital role in determining the applications of such materials in various fields including H_2 storage and CO_2 capture.[29,32−39,45−49]

CONCLUSIONS

We demonstrated a facile synthesis of core−shell ZIF-8@ZIF-67 and ZIF-67@ZIF-8 frameworks through a seed-mediated growth methodology. TEM, SEM, elemental mapping and line scan, PXRD, and XPS authenticated the core−shell topology of the studied ZIFs. ICP-AES analyses further evidenced an analogous Co-to-Zn composition for both the core−shell ZIFs. The observed remarkable enhancement in the H_2 storage properties of the core−shell ZIFs compared to either of the parent ZIF-8 and ZIF-67 clearly evidenced the coherent synergy between the core and the shell, along with the tuned porosity (surface area and pore volume) behavior of the synthesized core−shell ZIFs. Further, the poor H_2 storage properties of the physical mixture of ZIF-8 and ZIF-67 authenticated the crucial role of the core−shell morphology in achieving enhanced H_2 storage. Additionally, the synthesized core−shell ZIFs displayed improved CO_2 capture properties compared to ZIF-8 and ZIF-67. The observed unprecedented advanced properties displayed by the core−shell ZIFs for gas storage applications may present an opportunity to design new core−shell MOFs to achieve enhanced gas storage properties and several other advanced applications.

EXPERIMENTAL SECTION

Chemicals and Reagents. All chemicals and reagents were of analytical grade and used as delivered without further purification. These chemicals include Basolite Z1200 [2-methylimidazole zinc salt (ZIF-8), Sigma-Aldrich], cobalt (II) chloride hexahydrate [$CoCl_2{\cdot}6H_2O$, 97−102% assay (by complexometry), Loba Chemie], zinc nitrate hexahydrate [$Zn(NO_3)_2{\cdot}6H_2O$, ≥96.0% assay, Merck], polyvinylpyrrolidone (PVP) [$(C_6H_9NO)_n$, Sigma-Aldrich], and 2-methylimidazole [Hmim, 99% assay, Sigma-Aldrich]. Acetone [$(CH_3)_2CO$, ≥ 99%], methanol [CH_3OH, 99.7%], and distilled water were obtained from Merck. Highly pure certified He, N_2, CO_2, and H_2 gases used for the adsorption measurements were purchased from Inox air product Ltd., India.

Preparation of Core−Shell ZIF-8@ZIF-67 Framework. The core−shell framework of ZIF-8@ZIF-67 was fabricated via

DOI: 10.1021/acsomega.7b01693
ACS Omega 2018, 3, 167−175

adopting the seed-mediated growth method (Figure 1a) as followed by Yamauchi et al. with minor modifications.[36] In this work, commercially available Basolite Z1200 seeds (known as ZIF-8 purchased from Sigma-Aldrich) were utilized as the seed. Initially, 0.160 g of ZIF-8 seeds was dissolved in 20 mL of methanol under ultrasound for 20 min at ambient temperature. $CoCl_2{\cdot}6H_2O$ (0.354 g) and 1.790 g of 2-methylimidazole were separately dissolved in 6 mL of methanol solution. After forming a uniform solution of $CoCl_2{\cdot}6H_2O$ and 2-methylimidazole in methanol, the solution was stepwise injected into the core solution. Then, the mixture was stirred for another 20 min and transferred to a 50 mL Teflon-lined autoclave. The mixture was heated at 373 K for 12 h. The autoclave was allowed to cool to ambient temperature. The resultant ZIF-8@ZIF-67 solid was collected by centrifugation at 8000 rpm for 15 min. The obtained solid residue was washed several times with methanol, collected by centrifugation at 8000 rpm for 8 min, and dried under vacuum at 373 K overnight. Typical elemental analysis showed the following composition: C: 47.88 wt %; H: 5.49 wt %; and N: 22.64 wt %.

Preparation of Core−Shell ZIF-67@ZIF-8 Framework. The ZIF-67@ZIF-8 core−shell framework was prepared according to the earlier reported seed-mediated growth method (Figure 1a) by Li et al. with minor changes.[37] Initially, a homogenous methanolic solution of $CoCl_2{\cdot}6H_2O$ (1.092 g in 15 mL of methanol) and 2-methylimidazole (1.232 g in 30 mL of methanol) was prepared under ultrasonication for 2 min at 313 K. In the next step, a methanolic solution of $Zn(NO_3)_2{\cdot}6H_2O$ (1.116 g in 15 mL of methanol) was stepwise injected into the above-prepared core solution. Then, the mixture was ultrasonicated for 20 min at ambient temperature. Finally, the resultant solid of ZIF-67@ZIF-8 was collected via centrifugation at 8000 rpm for 15 min. The solid residue was washed several times with methanol, collected by centrifugation at 8000 rpm for 8 min, and dried under vacuum at 373 K overnight. Typical elemental analysis showed the following composition: C: 47.86 wt %; H: 5.39 wt %; and N: 22.73 wt %.

Preparation of ZIF-67 Framework. ZIF-67 [$Co(Hmim)_2$] was synthesized according to the previously reported procedure of Yamauchi et al.[36] $CoCl_2{\cdot}6H_2O$ (519 mg), 2630 mg of 2-methylimidazole, and 600 mg of PVP were first well-dispersed in 80 mL of methanol under stirring for 30 min at ambient temperature. Then, the reaction mixture was kept at ambient temperature for overnight. A bright purple mixture of ZIF-67 was collected by centrifugation at 8000 rpm for 15 min. The obtained solid residue was washed several times with methanol, collected by centrifugation at 8000 rpm for 8 min, and dried under vacuum at 373 K overnight.

Preparation of Physical Mixture of ZIF-8 and ZIF-67 Frameworks. A physical mixture of ZIF-8 and ZIF-67 was prepared by mixing the commercially available ZIF-8 and synthesized ZIF-67 in a Co/Zn molar ratio of 0.50 to meet results of ICP-AES analysis for ZIF-8@ZIF-67 (Co/Zn = 0.51) and ZIF-67@ZIF-8 (Co/Zn = 0.54). The physical mixture was further dried under vacuum at 373 K overnight.

Material Characterization. The PXRD pattern for the samples was obtained using a Rigaku SmartLab automated X-ray diffractometer system with monochromatic Cu $K\alpha_1$ radiation (λ = 1.540593 Å) at 40 kV and 30 mA. The diffraction angle was in the range of 5−40° with a scan speed of 3° per min and a scan step size 0.01°. TGA was carried out using a Mettler Toledo TGA/DSC1 instrument; approximately 8 mg of the samples was heated at a rate of 5 °C min^{-1} from room temperature to 800 °C. The morphology of the sample was characterized using a Carl Zeiss Supra-55 scanning electron microscope at an accelerating voltage of 5 kV. TEM (FEG-TEM) and EDXS measurements were carried out with the help of a JEOL instrument (JEM-2100F) at an operating voltage of 200 kV. Elemental mapping and line scan analysis were performed on an FEI Tecnai G2 F30 TEM with an operating voltage of 200 kV. The sample prepared for analysis was dispersed into methanol under ultrasound for 30 min. Then, the well-dispersed sample was spread over a carbon-coated Cu grid and dried at room temperature. ICP-AES technique was utilized to estimate the metal ion at a low level. ICP-AES analysis was conducted with the help of an ARCONS instrument, which synchronizes the ICP spectrometer (SPECTRO, Analytical Instruments GmbH, Germany) to the system. For the estimation of Zn^{2+} and Co^{2+} metal ions, the sample was digested into 20 mL of aqua regia solution. UV−vis spectra studies were performed on an Agilent Cary 60 spectrophotometer in the wavelength range 200−800 nm. The XPS analysis technique measured the electronic state of the elements present in a core−shell framework structure. XPS analysis was conducted with the help of an AXIS supra (Make: Kratos Analytical, UK) instrument. For XPS analysis, pellets of small size were made with the help of a mechanical press. The framework structure was dried at 393 K for 8 h under vacuum conditions before performing XPS measurement. Initially, a wide scan of survey spectrum was carried out at a pass energy of 160 eV and a resolution of 2 eV for the core−shell structure. To probe the electronic state of the main elements (Zn^{2+} and Co^{2+}), a high-resolution scan was performed at a pass energy of 20 and a resolution of 0.5 eV. The functional groups of the core−shell frameworks were identified by FT-IR using instruments of PerkinElmer Spectrum Version 10.5.1 in the 400−3000 cm^{-1} range of wavenumber. The samples were dried under vacuum conditions at 120 °C for 12 h before the FT-IR measurement. The elemental analysis of the core−shell framework was obtained using a Thermo Scientific analyzer. The N_2 adsorption−desorption isotherm of the samples was measured using a Qunatachrom Autosorb-iQ automated volumetric sorption instrument at 77 K. The BET and Langmuir surface areas were calculated in the relative pressure range of 0.05−0.25. The total pore volume was measured at the point P/P_0 = 0.99 using the N_2 adsorption−desorption isotherm data. The pore size distribution was estimated based on the NLDFT and BJH theory. The sample was outgassed at 393 K for 12 h under ultrahigh vacuum conditions before each measurement.

Evaluation of H_2 Storage and CO_2 Capture Performance. The H_2 storage and CO_2 capture adsorption isotherms for core−shell ZIF-8@ZIF-67 and ZIF-67@ZIF-8 along with the parent ZIF-8 and ZIF-67 and the physical mixture of ZIF-8 and ZIF-67 were measured using the static volumetric technique by an apparatus from Qunatachrome Autosorb-iQ. The low-pressure (up to 1 bar) H_2 gas adsorption isotherm was measured at 77 and 298 K, and CO_2 gas adsorption isotherm data were collected at 298 K. Before the gas adsorption measurements, the samples were dried at 393 K under vacuum for 12 h.

■ ASSOCIATED CONTENT

Supporting Information

The Supporting Information is available free of charge on the ACS Publications website at DOI: 10.1021/acsomega.7b01693.

DOI: 10.1021/acsomega.7b01693
ACS Omega 2018, 3, 167−175

Surface area calculation, adsorption equilibrium isotherm model, heat of adsorption, photographs of the synthesized core−shell ZIFs, SEM images, PXRD patterns, TEM images, EDXS plots, XPS analysis, elemental analysis, FT-IR spectra, TGA profiles, BET surface area, BJH pore size distribution, H_2 storage isotherm, Langmuir and Freundlich plots, H_2 storage isotherm, and CO_2 capture data (PDF)

AUTHOR INFORMATION

Corresponding Authors

*E-mail: anil@iiti.ac.in, anil@iittp.ac.in (E.A.K.).
*E-mail: sksingh@iiti.ac.in (S.K.S.).

ORCID

Sanjay K. Singh: 0000-0002-8070-7350

Notes

The authors declare no competing financial interest.

ACKNOWLEDGMENTS

This work was financially supported by IIT Indore, CSIR, New Delhi, and SERB (DST), New Delhi. D.K.P. and R.K.R. thank MHRD, Govt. of India, and IIT Indore, respectively, for their fellowships. Authors are grateful to SIC, IIT Indore, and SAIF, IIT Bombay, for the instrumentation facilities and IIT Indore for the extended research facilities. The authors also thank Prof. Pratibha Sharma, IIT Bombay, for her generous help in the characterization of ZIFs.

REFERENCES

(1) Turner, J. A. A Realizable Renewable Energy Future. *Science* **1999**, *285*, 687−689.
(2) Morris, R. E.; Wheatley, P. S. Gas Storage in Nanoporous Materials. *Angew. Chem., Int. Ed.* **2008**, *47*, 4966−4981.
(3) Schlapbach, L.; Züttel, A. Hydrogen-Storage Materials for Mobile Applications. *Nature* **2001**, *414*, 353−358.
(4) (a) Zhou, H.-C.; Long, J. R.; Yaghi, O. M. Introduction to Metal−Organic Frameworks. *Chem. Rev.* **2012**, *112*, 673−674. (b) Blanco, A. A. G.; Vallone, A. F.; Gil, A.; Sapag, K. A Comparative Study of Various Microporous Materials to Store Hydrogen by Physical Adsorption. *Int. J. Hydrogen Energy* **2012**, *37*, 14870−14880. (c) Rallapalli, P. B. S.; Raj, M. C.; Patil, D. V.; Prasanth, K. P.; Somani, R. S.; Bajaj, H. C. Activated Carbon@MIL-101(Cr): A Potential Metal-Organic Framework Composite Material for Hydrogen Storage. *Int. J. Energy Res.* **2013**, *37*, 746−753.
(5) (a) Furukawa, H.; Cordova, K. E.; O'Keeffe, M.; Yaghi, O. M. The Chemistry and Applications of Metal-Organic Frameworks. *Science* **2013**, *341*, 1230444. (b) Nandi, S.; Luna, P. D.; Daff, T. D.; Rother, J.; Liu, M.; Buchanan, W.; Hawari, A. I.; Woo, T. K.; Vaidhyanathan, R. A Single-ligand Ultra-microporous MOF for Precombustion CO_2 Capture and Hydrogen Purification. *Sci. Adv.* **2015**, *1*, No. e1500421.
(6) Chen, B.; Yang, Z.; Zhu, Y.; Xia, Y. Zeolitic Imidazolate Framework Materials: Recent Progress in Synthesis and Applications. *J. Mater. Chem. A* **2014**, *2*, 16811−16831.
(7) Eddaoudi, M.; Sava, D. F.; Eubank, J. F.; Adil, K.; Guillerm, V. Zeolite-Like Metal−Organic Frameworks (ZMOFs): Design, Synthesis, and Properties. *Chem. Soc. Rev.* **2015**, *44*, 228−249.
(8) Stock, N.; Biswas, S. Synthesis of Metal-Organic Frameworks (MOFs): Routes to Various MOF Topologies, Morphologies, and Composites. *Chem. Rev.* **2012**, *112*, 933−969.
(9) Park, K. S.; Ni, Z.; Cote, A. P.; Choi, J. Y.; Huang, R.; Uribe-Romo, F. J.; Chae, H. K.; O'Keeffe, M.; Yaghi, O. M. Exceptional Chemical and Thermal Stability of Zeolitic Imidazolate Frameworks. *Proc. Natl. Acad. Sci. U.S.A.* **2006**, *103*, 10186−10191.
(10) Hayashi, H.; Côté, A. P.; Furukawa, H.; O'Keeffe, M.; Yaghi, O. M. Zeolite A Imidazolate Frameworks. *Nat. Mater.* **2007**, *6*, 501−506.
(11) Wu, H.; Zhou, W.; Yildirim, T. Hydrogen Storage in a Prototypical Zeolitic Imidazolate Framework-8. *J. Am. Chem. Soc.* **2007**, *129*, 5314−5315.
(12) Banerjee, R.; Phan, A.; Wang, B.; Knobler, C.; Furukawa, H.; O'Keeffe, M.; Yaghi, O. M. High-Throughput Synthesis of Zeolitic Imidazolate Frameworks and Application to CO_2 Capture. *Science* **2008**, *319*, 939−943.
(13) Langmi, H. W.; Ren, J.; North, B.; Mathe, M.; Bessarabov, D. Hydrogen Storage in Metal-Organic Frameworks: A Review. *Electrochim. Acta* **2014**, *128*, 368−392.
(14) Sumida, K.; Rogow, D. L.; Mason, J. A.; McDonald, T. M.; Bloch, E. D.; Herm, Z. R.; Bae, T.-H.; Long, J. R. Carbon Dioxide Capture in Metal−Organic Frameworks. *Chem. Rev.* **2012**, *112*, 724−781.
(15) Bhattacharjee, S.; Jang, M.-S.; Kwon, H.-J.; Ahn, W.-S. Zeolitic Imidazolate Frameworks: Synthesis, Functionalization, and Catalytic/Adsorption Applications. *Catal. Surv. Asia* **2014**, *18*, 101−127.
(16) Lu, G.; Li, S.; Guo, Z.; Farha, O. K.; Hauser, B. G.; Qi, X.; Wang, Y.; Wang, X.; Han, S.; Liu, X.; DuChene, J. S.; Zhang, H.; Zhang, Q.; Chen, X.; Ma, J.; Loo, S. C. J.; Wei, W. D.; Yang, Y.; Hupp, J. T.; Huo, F. Imparting Functionality to a Metal−Organic Framework Material by Controlled Nanoparticle Encapsulation. *Nat. Chem.* **2012**, *4*, 310−316.
(17) Janiak, C.; Vieth, J. K. MOFS, Mils and More: Concepts, Properties and Applications for Porous Coordination Networks (PCNs). *New J. Chem.* **2010**, *34*, 2366−2388.
(18) Jiang, H.-L.; Liu, B.; Akita, T.; Haruta, M.; Sakurai, H.; Xu, Q. Au@ZIF-8: CO Oxidation over Gold Nanoparticles Deposited to Metal−Organic Framework. *J. Am. Chem. Soc.* **2009**, *131*, 11302−11303.
(19) Lu, G.; Hupp, J. T. Metal−Organic Frameworks as Sensors: A ZIF-8 Based Fabry−Pérot Device as a Selective Sensor for Chemical Vapors and Gases. *J. Am. Chem. Soc.* **2010**, *132*, 7832−7833.
(20) Shi, Q.; Chen, Z.; Song, Z.; Li, J.; Dong, J. Synthesis of ZIF-8 and ZIF-67 by Steam-Assisted Conversion and an Investigation of Their Tribological Behaviors. *Angew. Chem., Int. Ed.* **2011**, *50*, 672−675.
(21) Qian, J.; Sun, F.; Qin, L. Hydrothermal Synthesis of Zeolitic Imidazolate Framework-67 (ZIF-67) Nanocrystals. *Mater. Lett.* **2012**, *82*, 220−223.
(22) Tanabe, K. K.; Cohen, S. M. PostSynthetic Modification of Metal−Organic Frameworks—A Progress Report. *Chem. Soc. Rev.* **2011**, *40*, 498−519.
(23) Ahmed, I.; Jhung, S. H. Composites of Metal−Organic Frameworks: Preparation and Application in Adsorption. *Mater. Today* **2014**, *17*, 136−146.
(24) Liu, X.-W.; Sun, T.-J.; Hu, J.-L.; Wang, S.-D. Composites of Metal−Organic Frameworks and Carbon-Based Materials: Preparations, Functionalities and Applications. *J. Mater. Chem. A* **2016**, *4*, 3584−3616.
(25) Liu, J.; Thallapally, P. K.; McGrail, B. P.; Brown, D. R.; Liu, J. Progress in Adsorption-Based CO_2 Capture by Metal−Organic Frameworks. *Chem. Soc. Rev.* **2012**, *41*, 2308−2322.
(26) Botas, J. A.; Calleja, G.; Sánchez-Sánchez, M.; Orcajo, M. G. Cobalt Doping of the MOF-5 Framework and Its Effect on Gas-Adsorption Properties. *Langmuir* **2010**, *26*, 5300−5303.
(27) Lu, Y.; Zhou, Q.; Chen, L.; Zhan, W.; Xie, Z.; Kuang, Q.; Zheng, L. Templated Synthesis of Diluted Magnetic Semiconductors Using Transition Metal Ion-Doped Metal−Organic Frameworks: The Case of Co-Doped ZnO. *CrystEngComm* **2016**, *18*, 4121−4126.
(28) Tang, J.; Salunkhe, R. R.; Zhang, H.; Malgras, V.; Ahamad, T.; Alshehri, S. M.; Kobayashi, N.; Tominaka, S.; Ide, Y.; Kim, J. H.; Yamauchi, Y. Bimetallic Metal-Organic Frameworks for Controlled Catalytic Graphitization of Nanoporous Carbons. *Sci. Rep.* **2016**, *6*, 30295.
(29) Kaur, G.; Rai, R. K.; Tyagi, D.; Yao, X.; Li, P.-Z.; Yang, X.-C.; Zhao, Y.; Xu, Q.; Singh, S. K. Room-Temperature Synthesis of

DOI: 10.1021/acsomega.7b01693
ACS Omega 2018, 3, 167−175

Bimetallic Co−Zn Based Zeolitic Imidazolate Frameworks in Water for Enhanced CO_2 and H_2 Uptakes. *J. Mater. Chem. A* **2016**, *4*, 14932−14938.
(30) Zhou, K.; Mousavi, B.; Luo, Z.; Phatanasri, S.; Chaemchuen, S.; Verpoort, F. Characterization and Properties of Zn/Co Zeolitic Imidazolate Frameworks vs. ZIF-8 and ZIF-67. *J. Mater. Chem. A* **2017**, *5*, 952−957.
(31) Yang, X.; Xu, Q. Bimetallic Metal−Organic Frameworks for Gas Storage and Separation. *Cryst. Growth Des.* **2017**, *17*, 1450−1455.
(32) Hirai, K.; Furukawa, S.; Kondo, M.; Uehara, H.; Sakata, O.; Kitagawa, S. Sequential functionalization of porous coordination polymer crystals. *Angew. Chem., Int. Ed.* **2011**, *50*, 8057−8061.
(33) Li, T.; Sullivan, J. E.; Rosi, N. L. Design and Preparation of a Core−Shell Metal−Organic Framework for Selective CO2 Capture. *J. Am. Chem. Soc.* **2013**, *135*, 9984−9987.
(34) Koh, K.; Wong-Foy, A. G.; Matzger, A. j. MOF@MOF: Microporous Core−Shell Architectures. *Chem. Commun.* **2009**, 6162−6164.
(35) Szilágyi, P. Á.; Lutz, M.; Gascon, J.; Juan-Alcañiz, J.; van Esch, J.; Kapteijn, F.; Geerlings, H.; Dam, B.; van de Krol, R. MOF@MOF Core−Shell vs. Janus Particles and the Effect of Strain: Potential for Guest Sorption, Separation and Sequestration. *CrystEngComm* **2013**, *15*, 6003−6008.
(36) Tang, J.; Salunkhe, R. R.; Liu, J.; Torad, N. L.; Imura, M.; Furukawa, S.; Yamauchi, Y. Thermal Conversion of Core−Shell Metal−Organic Frameworks: A New Method for Selectively Functionalized Nanoporous Hybrid Carbon. *J. Am. Chem. Soc.* **2015**, *137*, 1572−1580.
(37) Yang, J.; Zhang, F.; Lu, H.; Hong, X.; Jiang, H.; Wu, Y.; Li, Y. Hollow Zn/Co ZIF Particles Derived from Core-Shell ZIF-67@ZIF-8 as Selective Catalyst for the Semi-Hydrogenation of Acetylene. *Angew. Chem., Int. Ed.* **2015**, *54*, 10889−10893.
(38) Zhang, J.; Zhang, T.; Xiao, K.; Cheng, S.; Qian, G.; Wang, Y.; Feng, Y. Novel and Facile Strategy for Controllable Synthesis of Multilayered Core−Shell Zeolitic Imidazolate Frameworks. *Cryst. Growth Des.* **2016**, *16*, 6494−6498.
(39) Ren, J.; Musyoka, N. M.; Langmi, H. W.; North, B. C.; Mathe, M.; Kang, X. Fabrication of Core−Shell MIL-101(Cr)@Uio-66(Zr) Nanocrystals for Hydrogen Storage. *Int. J. Hydrogen Energy* **2014**, *39*, 14912−14917.
(40) He, M.; Yao, J.; Liu, Q.; Wang, K.; Chen, F.; Wang, H. Facile Synthesis of Zeolitic Imidazolate Framework-8 from a Concentrated Aqueous Solution. *Microporous Mesoporous Mater.* **2014**, *184*, 55−60.
(41) (a) Butova, V. V.; Budnyk, A. P.; Bulanova, E. A.; Lamberti, C.; Soldatov, A. V. Hydrothermal Synthesis of High Surface Area ZIF-8 with Minimal use of TEA. *Solid State Sci.* **2017**, *69*, 13−21. (b) Eiras, D.; Labreche, Y.; Pessan, L. A. Ultem/ZIF-8 Mixed Matrix Membranes for Gas Separation: Transport and Physical Properties. *Mater. Res.* **2016**, *19*, 220−228. (c) Du, M.; Li, L.; Li, M.; Si, R. Adsorption Mechanism on Metal Organic Frameworks of Cu-BTC, Fe-BTC And ZIF-8 for CO_2 Capture Investigated by X-Ray Absorption Fine Structure. *RSC Adv.* **2016**, *6*, 62705−62716. (d) Peralta, D.; Chaplais, G.; Simon-Masseron, A.; Barthelet, K.; Pirngruber, G. D. Separation of C6 Paraffins Using Zeolitic Imidazolate Frameworks: Comparison with Zeolite 5A. *Ind. Eng. Chem. Res.* **2012**, *51*, 4692−4702. (e) Chen, H.; Wang, L.; Yang, J.; Yang, R. T. Investigation on Hydrogenation of Metal−Organic Frameworks HKUST-1, MIL-53, and ZIF-8 by Hydrogen Spillover. *J. Phys. Chem. C* **2013**, *117*, 7565−7576.
(42) (a) Zhou, W.; Wu, H.; Hartman, M. R.; Yildirim, T. Hydrogen and Methane Adsorption in Metal−Organic Frameworks: A High-Pressure Volumetric Study. *J. Phys. Chem. C* **2007**, *111*, 16131−16137. (b) Prabhakaran, P. K.; Deschamps, J. Doping Activated Carbon Incorporated Composite MIL-101 Using Lithium: Impact on Hydrogen Uptake. *J. Mater. Chem. A* **2015**, *3*, 7014−7021.
(43) Singh, V. K.; Kumar, E. A. Measurement and Analysis of Adsorption Isotherms of CO_2 on Activated Carbon. *Appl. Therm. Eng.* **2016**, *97*, 77−86.
(44) Foo, K. Y.; Hameed, B. H. Insights into the Modeling of Adsorption Isotherm Systems. *Chem. Eng. J.* **2010**, *156*, 2−10.
(45) Yang, S. J.; Cho, J. H.; Nahm, K. S.; Park, C. R. Enhanced Hydrogen Storage Capacity of Pt-loaded CNT@MOF-5 Hybrid Composites. *Int. J. Hydrogen Energy* **2010**, *35*, 13062−13067.
(46) Yang, S. J.; Choi, J. Y.; Chae, H. K.; Cho, J. H.; Nahm, K. S.; Park, C. R. Preparation and Enhanced Hydrostability and Hydrogen Storage Capacity of CNT@MOF-5 Hybrid Composite. *Chem. Mater.* **2009**, *21*, 1893−1897.
(47) Song, X.; Oh, M.; Lah, M. S. Hybrid Bimetallic Metal−Organic Frameworks: Modulation of the Framework Stability and Ultralarge CO2 Uptake Capacity. *Inorg. Chem.* **2013**, *52*, 10869−10876.
(48) Muhammad, R.; Rekha, P.; Mohanty, P. Aminal Linked Inorganic−Organic Hybrid Nanoporous Materials (HNMs) for CO_2 Capture and H_2 Storage Applications. *RSC Adv.* **2016**, *6*, 17100−17105.
(49) Rana, M. K.; Suffritti, G. B.; Demontis, P.; Masia, M. Simulation Study of CO_2 Adsorption Properties in Small Zeolite Imidazolate Frameworks. *Chem. Phys. Lett.* **2013**, *580*, 99−102.

DOI: 10.1021/acsomega.7b01693
ACS Omega 2018, 3, 167−175